Modeling the spatio-temporal variability in subsurface thermal regimes across a low-relief polygonal tundra landscape

Jitendra Kumar[1], Nathan Collier[2], Gautam Bisht[3], Richard T. Mills[4], Peter E. Thornton[1], Colleen M. Iversen[1], and Vladimir Romanovsky[5]

[1]Environmental Sciences Division, Oak Ridge National Laboratory, Oak Ridge, TN, USA
[2]Computer Science and Mathematics Division, Oak Ridge National Laboratory, Oak Ridge, TN, USA
[3]Lawrence Berkeley National Laboratory, Berkeley, CA, USA
[4]Intel Corporation, Hillsboro, OR, USA
[5]Geophysical Institute, University of Alaska Fairbanks, AK, USA

Correspondence to: Jitendra Kumar (jkumar@climatemodeling.org)

Abstract. Vast carbon stocks stored in permafrost soils of Arctic tundra are under risk of release to atmosphere under warming climate. Ice–wedge polygons in the low–gradient polygonal tundra create a complex mosaic of microtopographic features. The microtopography plays a critical role in regulating the fine scale variability in thermal and hydrological regimes in the polygonal tundra landscape underlain by continuous permafrost. Modeling of thermal regimes of this sensitive ecosystem is essential for understanding the landscape behavior under current as well as changing climate. We present here an end-to-end effort for high resolution numerical modeling of thermal hydrology at real–world field sites, utilizing the best available data to characterize and parameterize the models. We develop approaches to model the thermal hydrology of polygonal tundra and apply them at four study sites at Barrow, Alaska spanning across low to transitional to high-centered polygon, representing a broad polygonal tundra landscape. A multi–phase subsurface thermal hydrology model (PFLOTRAN) was developed and applied to study the thermal regimes at four sites. Using high resolution LiDAR DEM, microtopographic features of the landscape were characterized and represented in the high resolution model mesh. Best available soil data from field observations and literature was utilized to represent the complex heterogeneous subsurface in the numerical model. Simulation results demonstrate the ability of the developed modeling approach to model the complex thermal regimes across the sites. Our study provides insights into the critical role of polygonal tundra microtopography in regulating the thermal dynamics of the carbon rich permafrost soils. Study also highlights the importance of field–based observations of soil thermal and hydraulic properties for modeling–based studies of permafrost thermal dynamics and provides motivation for future observations by identifying gaps in our current understanding of the system.

1 Introduction

Coastal Arctic landscapes–dominated by wetlands and patterned ground–cover approximately 5–10% of Earth's land surface and play an important role in the hydrology, geomorphology, biogeochemistry and vegetation dynamics of the vast Arctic region. The low-gradient topography of the polygonal tundra characteristic of these landscapes is a complex mosaic of micro-

topographic features created by ice wedge polygons. This microtopography leads to strong fine–scale variability in thermal and hydrological regimes of landscapes underlain by continuous permafrost. Permafrost landforms like drained-lakes, low-centered polygons and high-centered polygons retard surface runoff after snowmelt, leading to increased surface water storage (in form of lakes, ponds and wetlands) (Kane et al. (2003)). Complex surface drainage patterns lead to heterogeneous soil moisture

5   and substrate conditions supporting a wide range of vegetation composition across the landscape. Arctic tundra soil pools are estimated to contain 190 Pg of carbon (Post et al. (1982)), much of which is under risk of rapid release to the atmosphere in a warming climate. Hobbie et al. (2000) studied the controls over carbon storage and turn-over in Arctic soils and found temperature, micro-topography and vegetation composition to be the primary controls at regional scale.

Changes in the surface geomorphology which lead to the creation of ice-wedge polygons are induced by thermal dise-

10 quilibrium and permafrost degradation. Lowland polygonal relief is dominated by low-centered polygons and high-centered polygons. Low-centered polygons are the most common polygonal landscape feature and are characteristic of poorly drained tundra. They consist of a raised rim with a wet central depression. Raised rims are the result of growing ice wedges that push material away from the center of the ice wedges to the sides (French (2007)). The standing water in the ice-wedge troughs leads to thermal erosion (i.e., accelerated thawing) along the rim. This preferential thaw may cause the ridge to collapse and

15 form trenches surrounding the polygon center, inverting the relief to form high-centered polygon. High-centered polygon are well-drained with often dry centers, leading to low peat accumulation and deeper active layers. The microtopographic relief and associated heterogeneity in soil moisture support a diverse distribution of vegetation in the Arctic, with wet centers and troughs of low-centered polygon covered by mosses and sedges, while drier rims, and centers of high-centered polygon and rims of low-centered polygon are dominated by mosses, lichen and dwarf shrubs. These diverse land-cover types can also

20 alter the surface energy balance and thermal properties through changes in albedo, surface roughness, and evapotranspiration (Langer et al. (2011)).

Large scale climate and terrestrial ecosystem processes are represented in global to regional scale climate and ecosystem models. However, most of these models lack the representation of fine scale heterogeneity in surface and subsurface processes at subgrid scale that exercise significant control on the landscape scale behavior. Representation of the fine scale heterogeneity

25 is important to model the non-linear processes involved (Aleina et al. (2013)).

Accurate characterization and modeling of subsurface thermal regimes in polygonal tundra is critical for our understanding of this sensitive system and our ability to predict its fate under climate change. In this study we developed approaches to 1) characterize the surface microtopography and subsurface structure of the polygonal tundra, 2) represent heterogeneous subsurface stratigraphy and hydraulic and thermal properties, 3) numerically model permafrost hydrology, and 4) combine the

30 above to simulate the permafrost thermal regime at field sites in a polygonal tundra region near Barrow, Alaska.

2   Study Area

The study area is located within the Barrow Environmental Observatory (BEO), (Figure 1) which lies 6 km East of Barrow, Alaska (71°18'N, 156°35'W), and is a field site of the U.S. Department of Energy's Next Generation Ecosystem Experiments

(NGEE) – Arctic project. The BEO spans 32.21 km^2 of natural tundra, lakes, and wetlands, and is reserved for scientific research. The landscape has low topographic relief, with elevations ranging from 0 to 7 m above sea level and low hydraulic gradient present across the region. Barrow has a polar maritime climate with mean annual air temperature of -12.0$°C$ and 3.3$°C$ during summer (June – August) (Liljedahl et al. (2011)). The winter snowpack averages 20 to 40 cm, but snow accumulation

5   is spatially variable due to variations in terrain roughness and drifting from strong easterly winds (Bockheim et al. (2001)). Annual adjusted precipitation is 173 mm, with the majority of precipitation falling during summer months (Liljedahl et al. (2011)). The polygonal tundra landscape is punctuated by thermokarst lakes and drained lake basins, with grass, moss, and sedge as dominant vegetation types. Basins at Barrow are underlain by permafrost within 1 m of the surface and are classified as Gelisols, with an organic-rich surface layer underlain by a horizon of silt and clay to silt-loam textured mineral material and

10   a frozen organic-rich mineral layer (Bockheim et al. (2001)). The seasonal active layer thickness ranges between 30 to 70 cm at the BEO.

    The various stages of geomorphologial and ecological change from low to transitional to high-centered polygon, lakes and drained lakes are all represented at the BEO. Following a "space for time" philosophy, NGEE–Arctic intensive field sites at BEO were chosen across the landscape to observe and study polygonal landscapes at all stages of transition. Table 1 shows the

15   characteristics of four sites (A, B, C, D) where our current study is focused.

Table 1. Areas A, B, C, D polygonal features and environmental characteristics.

Area	Characteristics	Relative Elevation (Min / Max / Median m)
A	Low center polygons (with ridges and troughs)	Low (4.5 / 4.9 / 4.6)
B	High center polygons	High (4.5 / 5.1 / 4.8)
C	Transitional low center polygons (with ridges and troughs)	Moderate (4.3 / 4.9 / 4.6)
D	Low center polygons (no troughs)	Low (4.1 / 4.6 / 4.3)

Relative elevation is qualitative summary of topography in the region, while Min/Max/Median are minimum, maximum and median elevations.

    A suite of observations are being collected at each of these intensive sites. Since 2012, meteorological data (including air temperature, summer precipitation, snow depth, relative humidity, wind speed and radiation) are being collected at all four sites (Hinzman et al. (2014b)). Surface temperature data is being collected along a transect from the center of the polygon to ridge to trough. Each location on the transect consists of nine soil temperature sensors ranging in depth from 2 cm to 150 cm

20   (Romanovsky and Cable (2012) http://lapland.gi.alaskaedu/vdv/index.html). Figure 2 shows the observed time series of hourly air temperature and liquid precipitation at our four sites for the period of October 1, 2013 – September 30, 2014. Data for the one year period (October 1, 2013 – September 30, 2014) were chosen for this study since it was only complete year for which all the necessary observations were available. Figure 3 shows high resolution imagery of the sites where the observations have been collected. Figure 3 shows the boundary of the region around the intensive sites where we conducted the detailed modeling

25   study presented here.
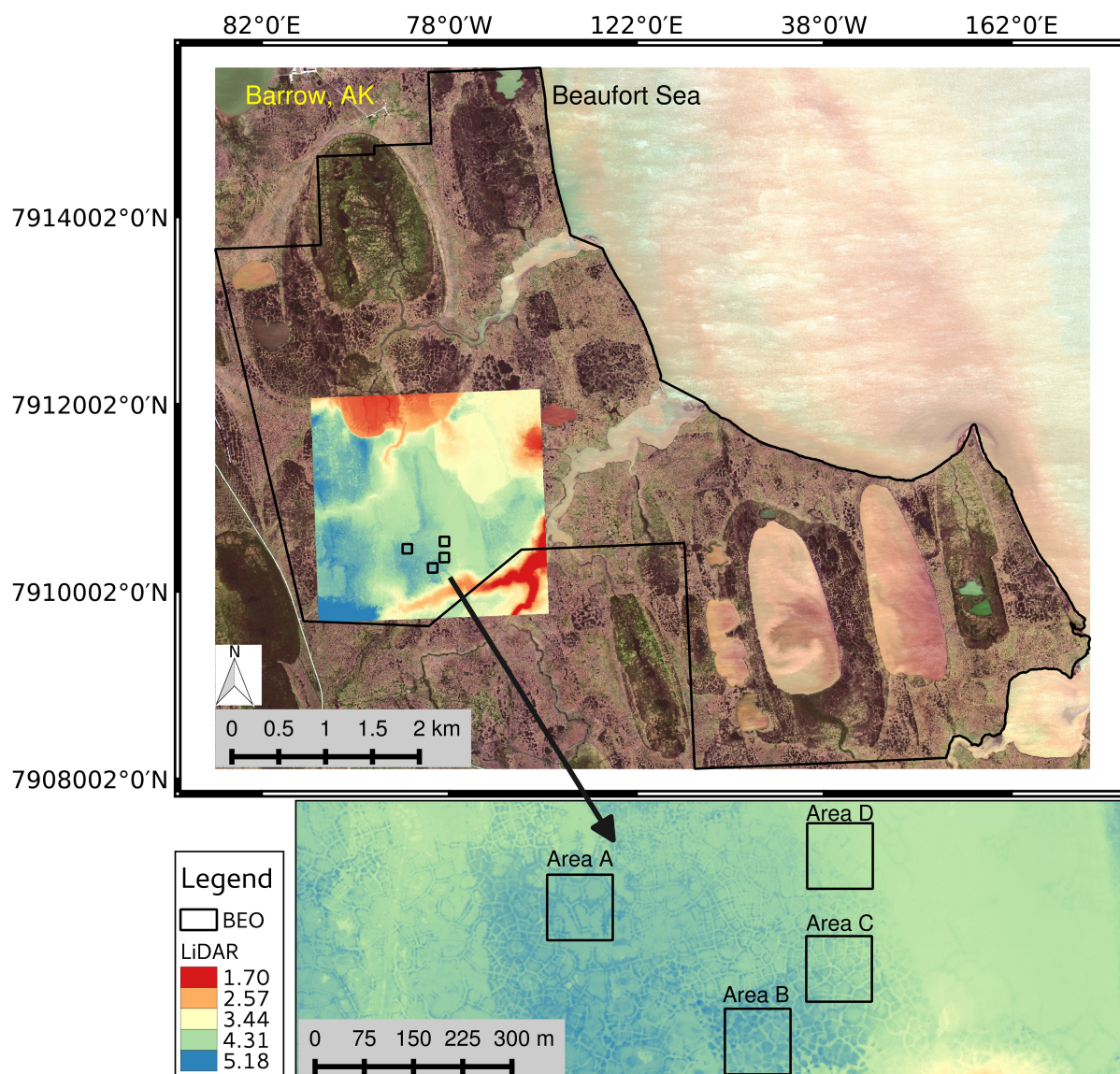
Figure 1. NGEE-Arctic Field Sites at BEO

(a) Site A

(b) Site B

(c) Site C

(d) Site D

Figure 2. Meteorological conditions at study sites. Red lines: hourly air temperature, Blue histograms: hourly summer time liquid precipitation
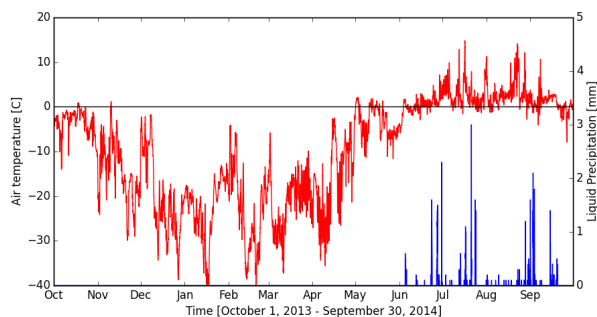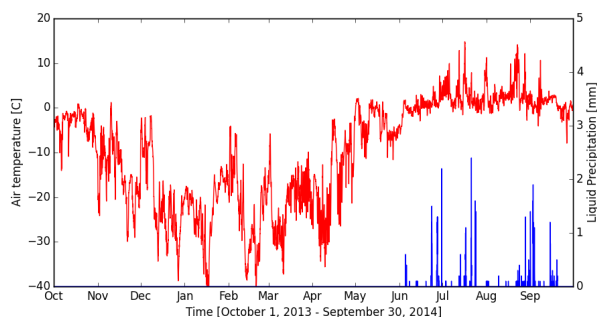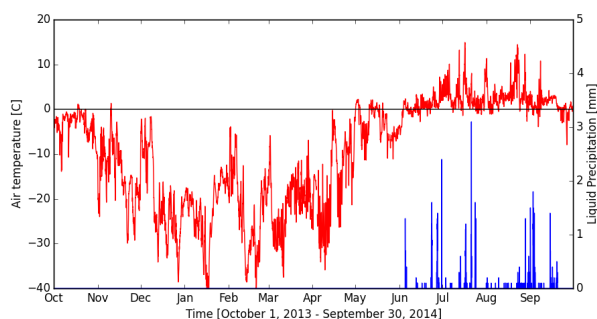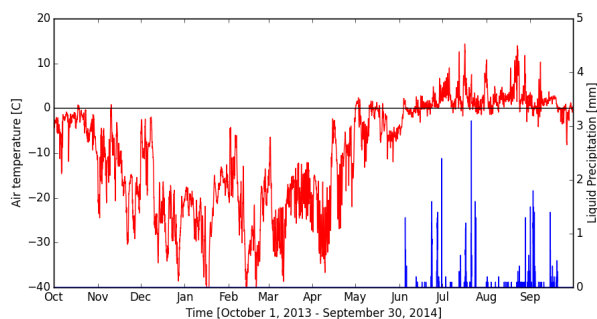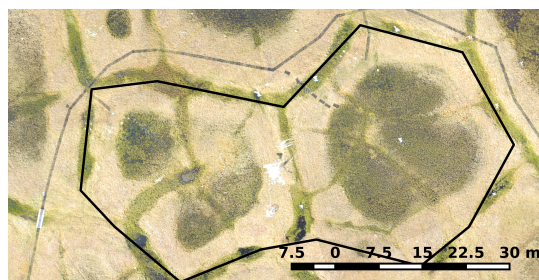
(a) Site A
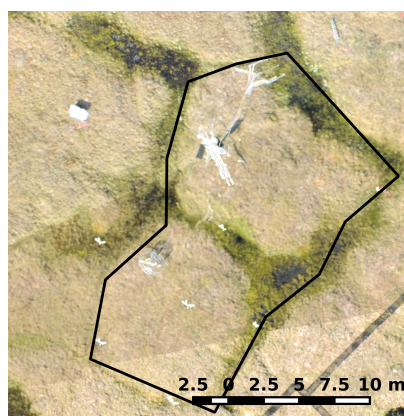
(b) Site B

(c) Site C
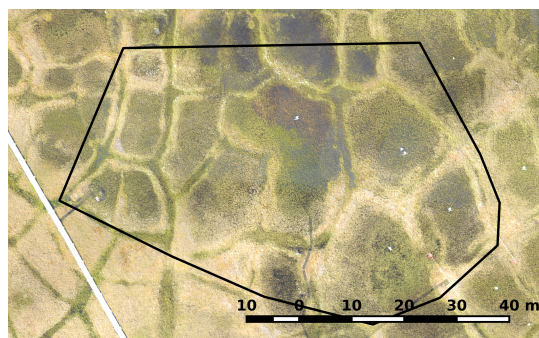
(d) Site D

Figure 3. Aerial imagery of the study areas at Sites A, B, C, D.

3 Methodology

To model the thermal regimes of the heterogeneous polygonal tundra ecosystem we developed approaches to 1) characterize the surface microtopography and subsurface structure of the polygonal tundra 2) represent heterogeneous subsurface stratigraphy and hydraulic and thermal properties, and 3) numerically model permafrost hydrology.

3.1 Representation of landscape heterogeneity

Accurate representation of polygonal tundra in the model requires 1) identification of microtopographic features on the landscape and 2) characterization of soil stratigraphy and properties across the landscape.

3.1.1 Identification of polygonal features

The human eye can discern polygonal patterns and features in satellite high resolution satellite imagery with relative ease. However, automated recognition and delineation of such features are challenging due to the variability in their spectral appearance, irregularity of polygon shape, dimension and orientation and lack of unique spectral signatures associated with the features (Skurikhin et al. (2013)). Muster et al. (2012) investigated the subpixel heterogeneity in Landsat satellite imagery over ice-wedge polygonal tundra using a range of multi-scale data (field measurements and remote sensing) and concluded that resolutions of 4 m or less are necessary to map the fine-scale landscape elements of polygonal tundra. Skurikhin et al. (2013) used a combination of segmentation and shape-based classification approaches using high-resolution WorldView-2 satellite imagery (60 cm resolution) to identify the landscape elements within the BEO. While they reported an overall accuracy of 95%, their study region was limited to a 1000×1100 pixels subimage. The scalability of such a specialized algorithm based on high-resolution satellite imagery (of limited availability) is untested and difficult for application for landscape–scale studies like ours.

Thus, with landscape–scale application in mind, we employed a relatively simple and generic approach using a high resolution Digital Elevation Model (DEM) that exploits the relative difference in surface elevations that distinguish the polygonal features (center, ridges and troughs). High-resolution LiDAR data (25 cm resolution) were collected on October 4, 2005 by Dr. Craig Tweedie of the University of Texas, El Paso. The LiDAR data horizontal and vertical accuracy were approximately 30 and 15 cm respectively. Covering an approximately 2.5 $km \times$ 2.5 km area, the data set encompasses all of the NGEE-Arctic intensive sampling sites (Figure 1) where our study was focused. Using a high resolution DEM created from this data set, elevation contours (10 cm interval) were developed to segment and classify the landscape in centers, ridges and troughs.

- _Site A_: Elevation at Site A ranged from a minimum of 4.5 m to a maximum of 4.9 m (Figure 4(a)). Low elevation depressions (4.5 – 4.6 m) were classified as Center, surrounded by elevated rim (4.7 – 4.9 m), and deep troughs adjacent to them (4.6 – 4.7 m). Center, Rim and Troughs occupied approximately 35%, 24% and 41% area respectively (Figure 4(b)).

- *Site B*: At Site B with high-centered polygons, elevation ranges from $4.5 - 5.1$ m (Figure 4(c)). High elevation areas ($4.8 - 5.1$ m) were classified as Center, low elevation ($4.7 - 4.8$ m) rim and deep troughs ($4.5 - 4.7$ m), occupying 39%, 21%, and 40% of total area respectively (Figure 4(d)).

- *Site C*: A wider range ($4.3 - 4.9$ m) of elevations are present at Site C (Figure 4(e)) which are often considered *low* or flat-centered polygon. Low elevation areas ($4.5 - 4.6$ m) were classified as Center, with raised rims ($4.6 - 4.9$ m) and deep ($4.3 - 4.5$ m) troughs. Center, Rim and Trough occupied 35%, 36%, and 29% of the total area (Figure 4(f)).

- *Site D*: Site D is relatively flat and is thus identified as flat-centered polygons, with the entire area within a narrow elevation range of $4.1 - 4.6$ m. While polygonal features were evident in 0.25 m resolution aerial optical image (Figure 3(d)), they were difficult to identify in the LiDAR DEM (Figure 4(g)) due to the limitations of the vertical accuracy of LiDAR. Trough features in flat-centered polygons are not well pronounced. Thus the area was classified only as Center ($4.1 - 4.3$ m) and Rim ($4.3 - 4.6$ m) features. About 72% of the area was classified as Center while 28% as Rim (Figure 4(h)).

We did not apply any specialized rules to enforce any shape, dimension and/or patterns of the polygon features (Center, Ridge, Trough), allowing us to scale our approach to the entire region where high resolution DEMs were available.

3.1.2 Subsurface characterization

The structure and properties of subsurface soils are important factors controlling the pattern and variability of permafrost thermal processes in the tundra environment, and accurate characterization and representation of the heterogeneous subsurface properties is critical to understanding and modeling the subsurface thermal dynamics. However, the limited availability of soil properties in tundra environments and at our sites at the BEO presents a significant challenge.

During the period July 31 – August 3, 2012 a field campaign was conducted by NGEE-Arctic researchers to collect soil cores at one replicate polygon at each of the sites A, B, C, and D at three micro-topographic positions (Center, Ridge, Trough) per polygon. Cores were collected using a hammer and a 5.08 cm diameter corer to collect one soil core per location to a depth of 30 cm. The soil horizons (moss, organic layer, mineral layer) were measured for each core to the nearest centimeter. A deep organic layer was found at several of the locations. However the total depth of the deep organic layer was not determined if it extended beyond the 30 cm core depth. Cores were collected for the purpose of biogeochemical analysis and thus no soil hydraulic or thermal properties were measured by the team. Figure 5 illustrates the subsurface soil horizons based on observations that we used in all our modeling studies presented here. In absence of co-located observations for soil hydraulic and thermal properties we derived the data for use in our studies from the published literature in tundra regions (Hinzman et al. (1991),Hinzman et al. (1998)) and a recent parameter calibration study conducted at one of our sites (site C) (Atchley et al. (2015)). Table 6 shows the soil hydraulic and thermal properties used in our modeling study.

3.1.3 Development of microtopography resolving computational mesh

Collier and Kumar (2016) developed MeshMaker, a Python-based meshing framework to create high resolution computational meshes for use in numerical simulation of permafrost thermal hydrologic processes at our polygonal tundra study sites. The
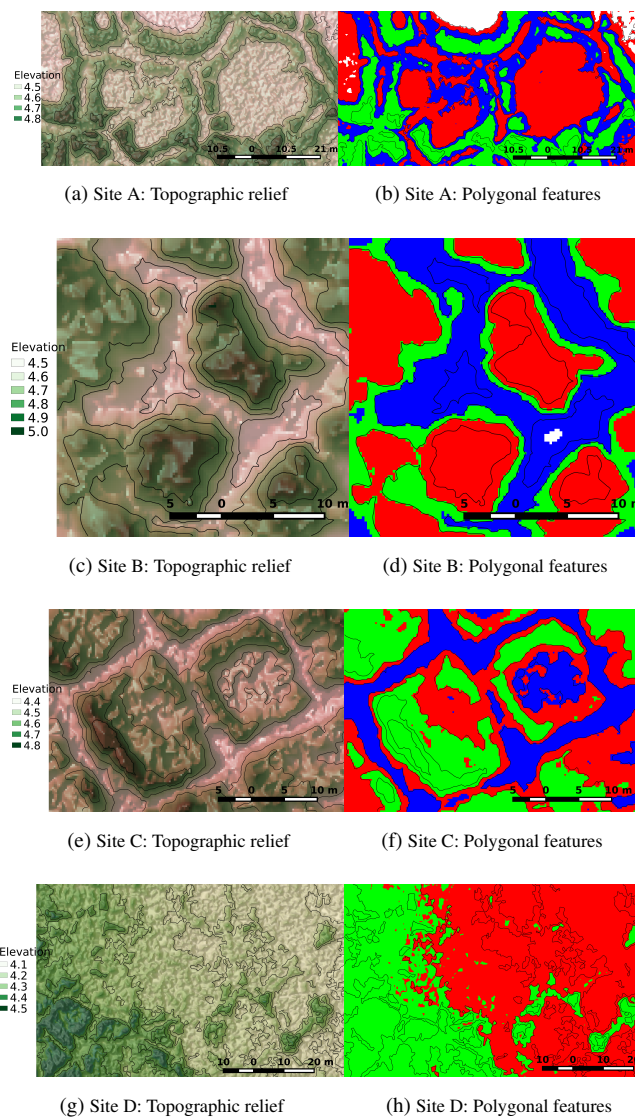
Figure 4. Elevation contour based classification of the study areas at Sites A, B, C, D. In subfigures (b,d,f, and h) the colors reflect polygon type (red: center; green: ridge; blue: trough).
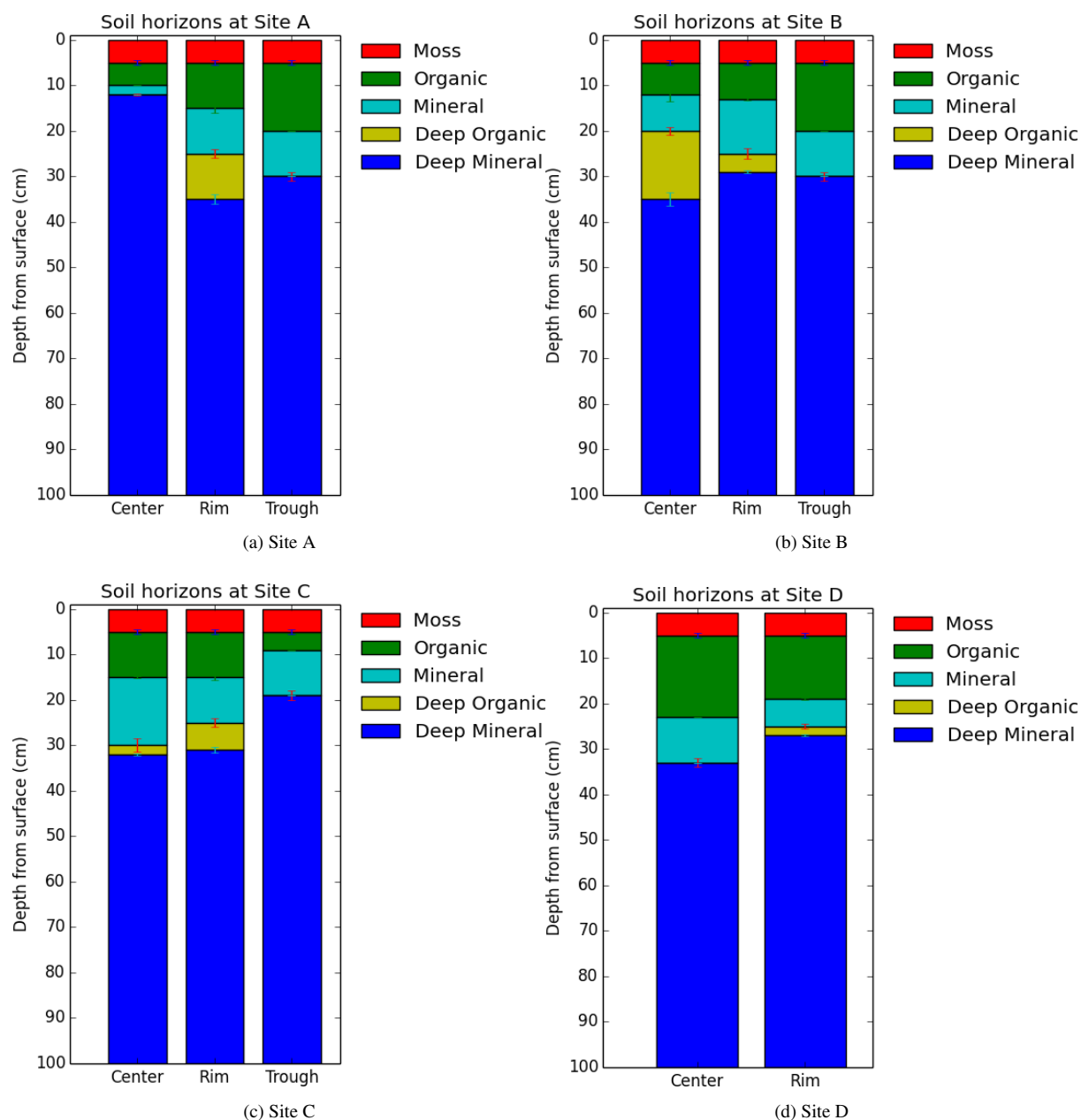
Figure 5. Subsurface soil horizons across microtopographic positions at Sites A, B, C, D.

meshing framework uses a high-resolution DEM and landscape classification (Figure 4) to develop Triangulated Irregular Networks (TINs). Non-uniform locally refined TINs adapt to the topographic complexity to create fine-resolution elements in areas with sharp changes in topography while creating coarser elements elsewhere, thus creating a high quality micro-topography resolving mesh (Figure 7).

5   Data from Sections 3.1.1 and 3.1.2 were embedded within the generated meshes (Figure 6) to represent the heterogeneity in the thermal hydrology models. By overlaying the TIN mesh with classified maps from Section 3.1.1, micro-topographic position (Center/Ridge/Trough of a polygon) of each element in the mesh was identified. Polygon type and micro-topographic specific soil horizons data (Section 3.1.2) were used to determine the soil horizons in the model mesh. While our data set was limited to a single replicate for each polygon type and location, significant spatial heterogeneity exists in reality. We assumed

10 a variability of 10% in soil horizon (moss, organic, mineral and deep organic soil) depths and stochastically generated the soil horizon depths at each spatial location in the modeling domain.

3.2 Three phase model for permafrost hydrology

In this study, we will use the open–source code PFLOTRAN to model the flow of mass and energy in the subsurface. PFLO-TRAN (Hammond et al. (2016, 2014)) is a state-of-the-art, massively parallel subsurface flow and reactive transport code.

15 PFLOTRAN solves a system of generally nonlinear partial differential equations (PDEs) describing multiphase, multicomponent and multiscale reactive flow and transport in porous materials. One system of PDEs which PFLOTRAN implements is a three-phase, thermal-hydrology model (the TH process model in PFLOTRAN parlance) which describes a balance of mass

$$\frac{\partial}{\partial t}\left[\varphi\left(s_\ell\eta_\ell + s_i\eta_i + s_g\eta_g\right)\right] + \nabla\cdot(\eta_\ell\mathbf{q}_\ell) = Q_M \tag{1}$$

and energy,

$$\frac{\partial}{\partial t}\left[\varphi\left(s_\ell\eta_\ell U_\ell + s_i\eta_i U_i + s_g\eta_g U_g\right) + (1-\varphi)\rho_s c_s T\right]$$
$$+\nabla\cdot(\eta_\ell\mathbf{q}_\ell H_\ell - \kappa_{eff}\nabla T) = Q_E \tag{2}$$

in which the liquid pressure P_ℓ and the bulk temperature T are the unknown variables. In equations (1) and (2), φ refers to porosity, s to percent saturation, η to molar density, U to internal energy, ρ to mass density, c to specific heat, and H to enthalpy. The subscripts $\{\ell, g, i\}$ refer to the liquid, gas, and ice phases of water, respectively, and the subscript s to the soil matrix. The

25 Darcy velocity is given by,

$$\mathbf{q}_\ell = -\frac{kk_r}{\mu_\ell}\nabla\left(P_\ell - \rho_\ell gz\right) \tag{3}$$

where k denotes intrinsic permeability, k_r relative permeability, μ viscosity, g unsigned gravity, and z the vertical component of the position vector $\mathbf{x}$. The effective thermal conductivity is expressed as

$$\kappa_{eff} = K_i\kappa_i + K_\ell\kappa_\ell + (1 - K_i - K_\ell)\kappa_g \tag{4}$$
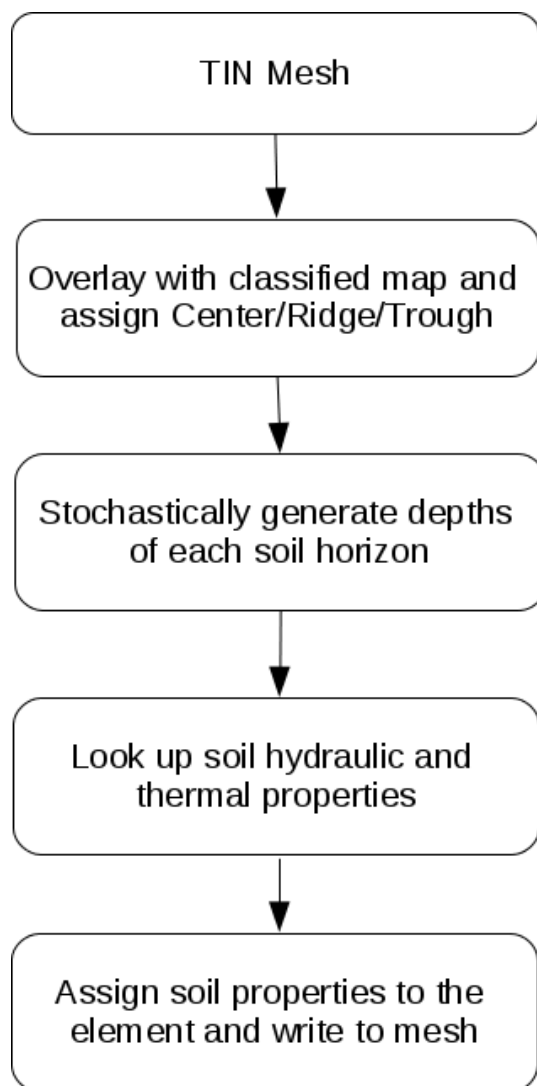
Figure 6. Workflow for heterogeneous soil parameter assignment in the computational mesh.

(a) Site A   (b) Site B

(c) Site C   (d) Site D
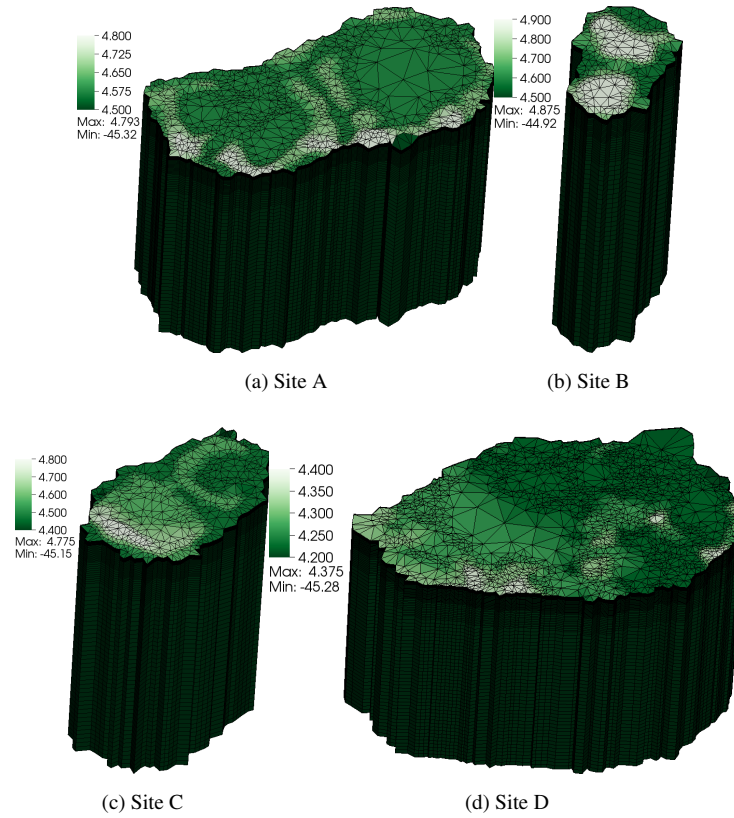
Figure 7. Microtopography resolving unstructured meshes. The coloring reflects the ground surface elevation.

where κ are the thermal conductivities of each pure phase and K represents the Kersten number of the frozen and unfrozen phase,

$$K_i = (s_i + \epsilon)^{\alpha_i} \tag{5}$$

$$K_\ell = (s_\ell + \epsilon)^{\alpha_\ell} \tag{6}$$

5   where $\epsilon = 1 \times 10^{-6}$ and α_i and α_ℓ are parameters of the assumed power law. The variables Q_M and Q_E represent generic mass and energy sources and sinks. We emphasize that the saturations, densities, and internal energies are all nonlinear functions of the liquid pressure and temperature and include the latent heat of fusion associated with change of phase. We also note that PFLOTRAN implements several choices of constitutive models for relating the saturations to the liquid pressure and bulk temperature. For more details on the formulation, see Painter (2011), Painter and Karra (2014), and Karra et al. (2014).

4 Modeling permafrost thermal hydrology

4.1 Initial and boundary conditions

3-D subsurface models for each of the four sites were initialized by freezing the entire modeling domain at a temperature of -1.0 °C. The models were spun up to a thermal periodic steady state using a time series of mean daily temperatures applied to the

5 top of the domain (ground surface). Mean daily near-surface temperature time series for period October 1, 2013 – September 30, 2014 were derived from hourly in situ temperatures from sensors located at 2 cm depths. At all four sites, using sensors installed at center, ridge and troughs, three different time series were prepared. Using the classification (center, ridge, trough) embedded in the model (Section 3.1.1), these micro-topography specific temperature time series were applied in a spatially heterogeneous, micro-topography aware manner to simulate the complex thermal hydrologic regimes in permafrost soils at

10 the BEO. A no–flow boundary condition was applied to the sides of the domain, while the deep bottom boundary was held at constant -10 °C, based on the temperature from West Dock site (Figure 3 of Romanovsky et al. (2010)) which is located at a comparable latitude (70.4°N) to the BEO (71.29°N). Surface processes (such as vegetation cover and snow) play an important role in regulating the thermal regimes of permafrost soils. While the surface processes are not represented in our model, use of near ground surface (2 cm depth) temperature as the boundary condition for the simulation allows us to isolate the effect of

15 surface processes.

4.2 Simulation of permafrost thermal regimes

After the models were spun up to periodic steady state condition, the simulation was continued for another year and outputs were used for validation and analysis. Soil temperature observations from the thermal sensors at 2 cm depths at the sites for the period October 1, 2013 – September 30, 2014 were used to drive the time dependent (Dirichlet) boundary condition at

20 the top (ground surface) of the model. In addition, mean daily time series (October 1, 2013 – September 30, 2014) of liquid (summer time) precipitation was also applied as moisture input to the model. Groundwater infiltration was considered to be zero if ground surface temperature was below freezing or if the domain was fully saturated. While soil moisture plays an important role, the focus of this study was on thermal hydrology and thus all results and discussions presented are focused on soil temperature. Soil temperature data from all the sensors (nine sensors at depths from 5 cm to 150 cm) were used to evaluate

25 the accuracy of the models.

At all the sites, simulated soil temperatures in the top most soil layer (5 cm thick) compared well with the observed near surface temperature at 5 cm depth (Figures 8(a),9(a),10(a),11(a)). Simulated soil temperatures in deeper soils were also in good agreement with the observed temperatures at the sensors (coefficient of determination R^2 0.93 – 0.99) (Tables 2,3,4,5). Model matched the observations with a Root Mean Square Error ($RMSE$) of 0.60 – 0.99 °C near surface, with an increasing

30 errors at deeper soils. While modeled temperature bias was in range of -0.30 – 0.10 °C near surface, a warm bias of up to 1.0 – 1.8 °C was found at deep soils.

Figures 8,9,10,11 shows the comparison between the simulated and observed soil temperatures at several select depths (5 cm, 10 cm, 20 cm, 50 cm, 100 cm and 150 cm from surface) at sites A, B, C, and D respectively. Simulated temperatures across

(a) Depth = 5 cm

(b) Depth = 10 cm

(c) Depth = 20 cm

(d) Depth = 50 cm

(e) Depth = 100 cm

(f) Depth = 150 cm
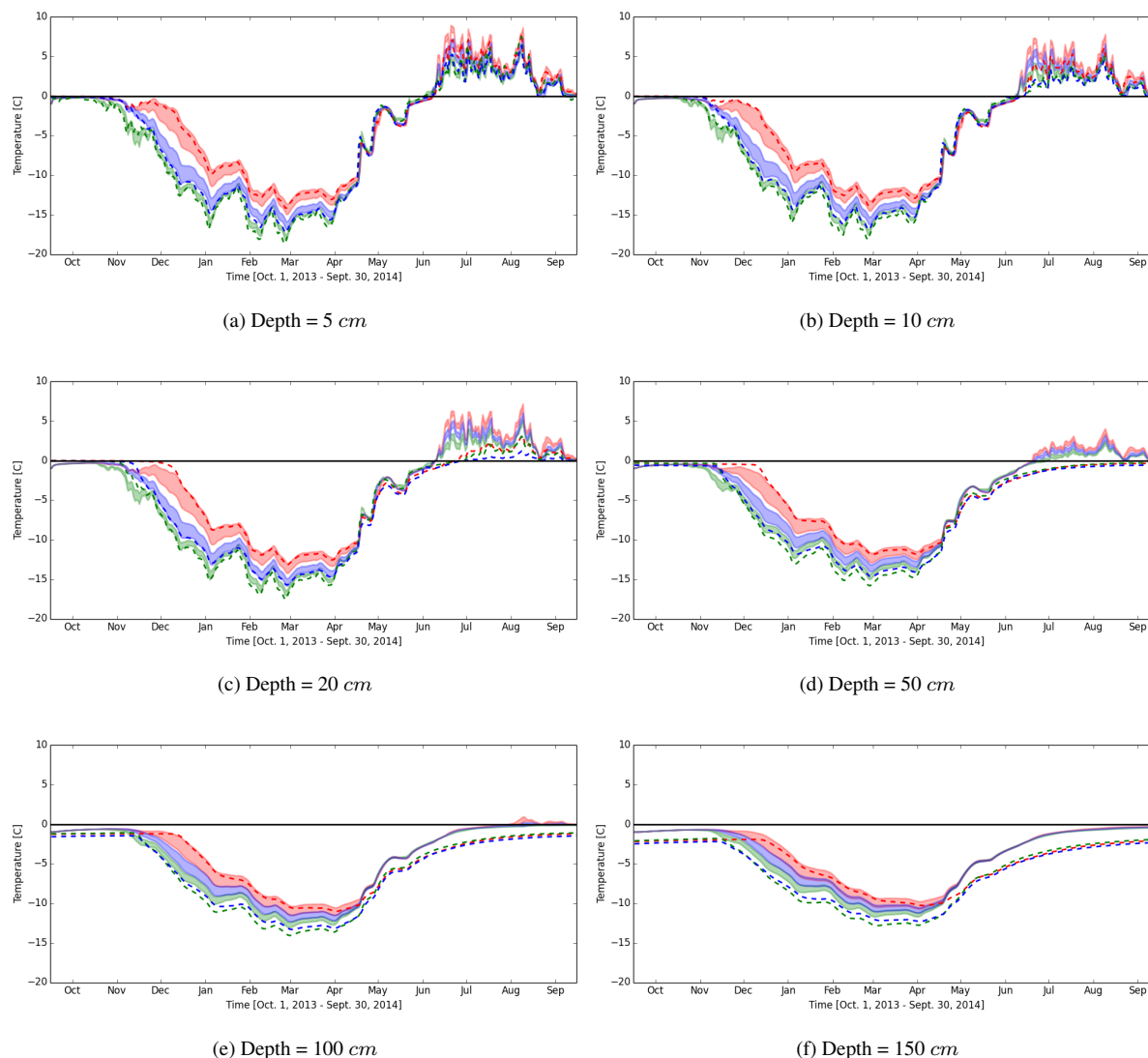
Figure 8. Simulated vs observed soil temperatures at Site A

(dotted lines represent observed data at center (in red), rim (green), and trough (blue) locations, while shaded curves show mean +/- standard deviation of simulated daily soil temperatures across the domain.
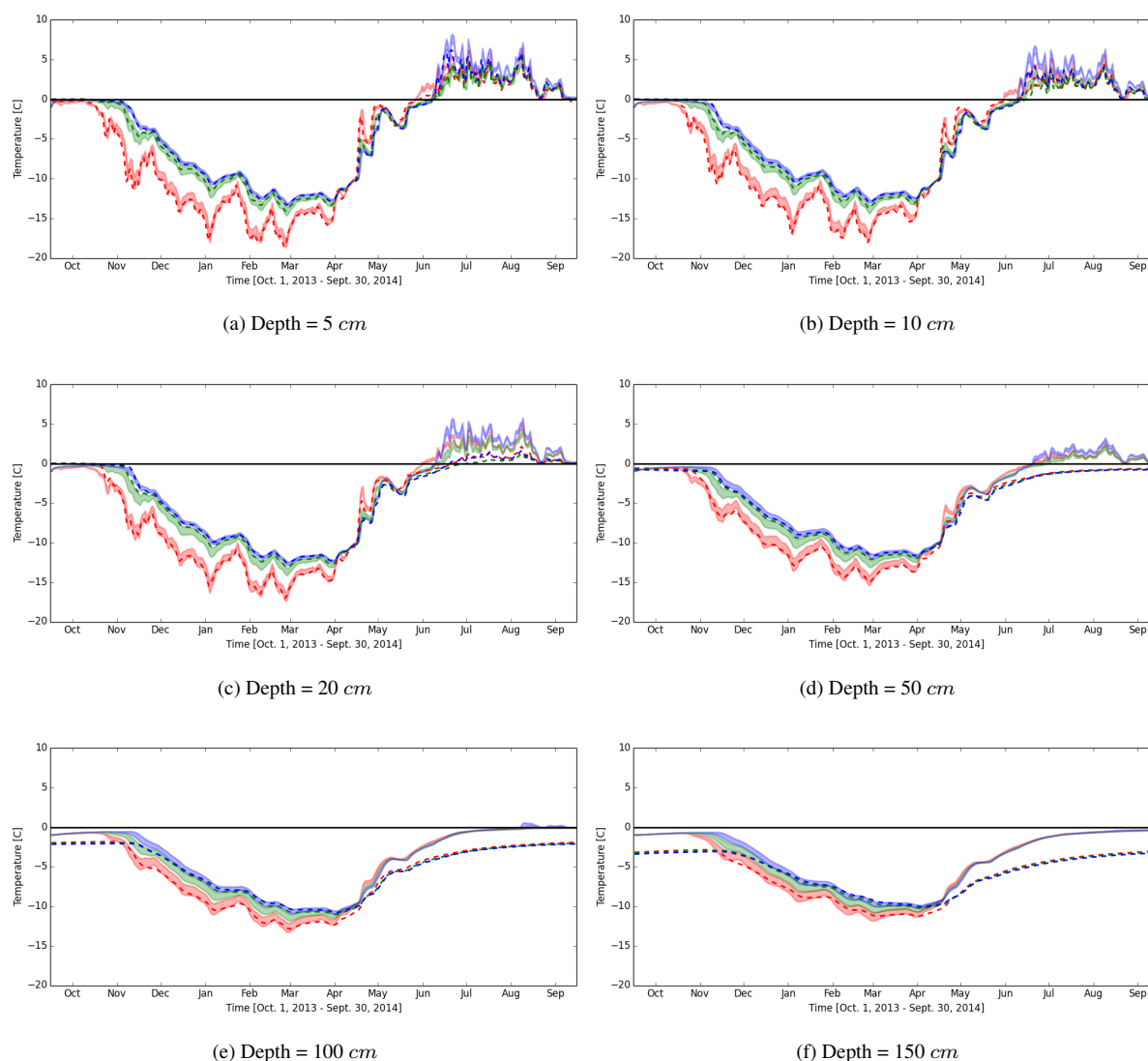
Figure 9. Simulated vs observed soil temperatures at Site B

(dotted lines represent observed data at center (in red), rim (green), and trough (blue) locations, while shaded curves show mean +/- standard deviation of simulated daily soil temperatures across the domain.

all the sites matched very well with the observed temperatures at shallow depths, but showed a deviation towards warmer than observed temperatures in deep soils. With soil cores collected at the sites limited to top 30 cm of the soil, our understanding of structure and physical and thermal properties of deeper soils is limited. For example, while we know that presence of ground ice (like ice wedges, segregated ice, ice lens etc.) is common in subsurface of Arctic tundra, their representation in the model

5   is completely missing. While PFLOTRAN has the ability to capture and model such cryostructures, we lack any quantitative data to characterize them for representation in the model.
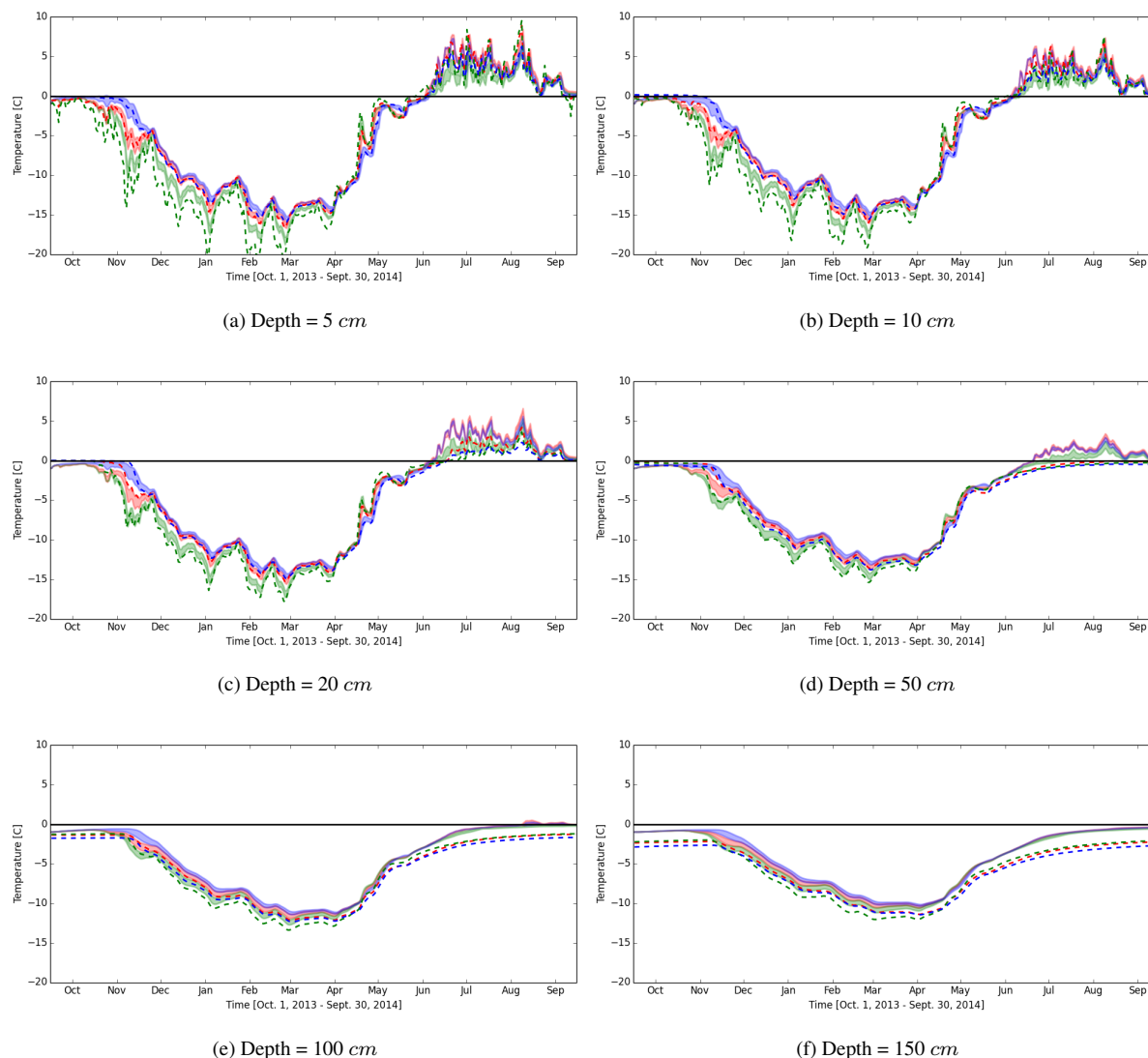
Figure 10. Simulated vs observed soil temperatures at Site C

(dotted lines represent observed data at center (in red), rim (green), and trough (blue) locations, while shaded curves show mean +/- standard deviation of simulated daily soil temperatures across the domain.

(a) Depth = 5 cm

(b) Depth = 10 cm

(c) Depth = 20 cm

(d) Depth = 50 cm

(e) Depth = 100 cm

(f) Depth = 150 cm
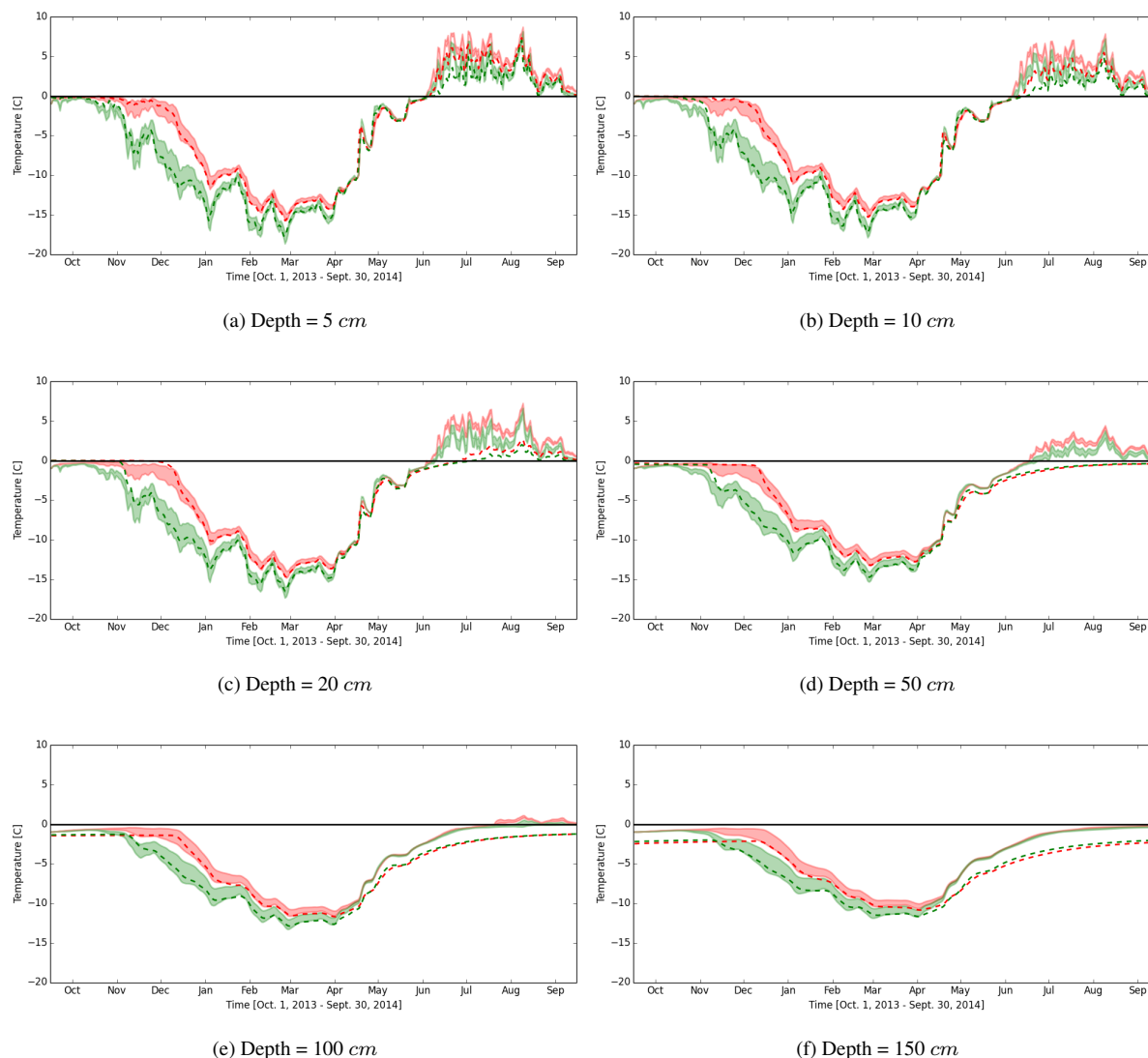
Figure 11. Simulated vs observed soil temperatures at Site D

(dotted lines represent observed data at center (in red), rim (green), and trough (blue) locations, while shaded curves show mean +/- standard deviation of simulated daily soil temperatures across the domain.

(a) Depth = 5 cm

(b) Depth = 10 cm

(c) Depth = 20 cm

(d) Depth = 50 cm

(e) Depth = 100 cm

(f) Depth = 150 cm
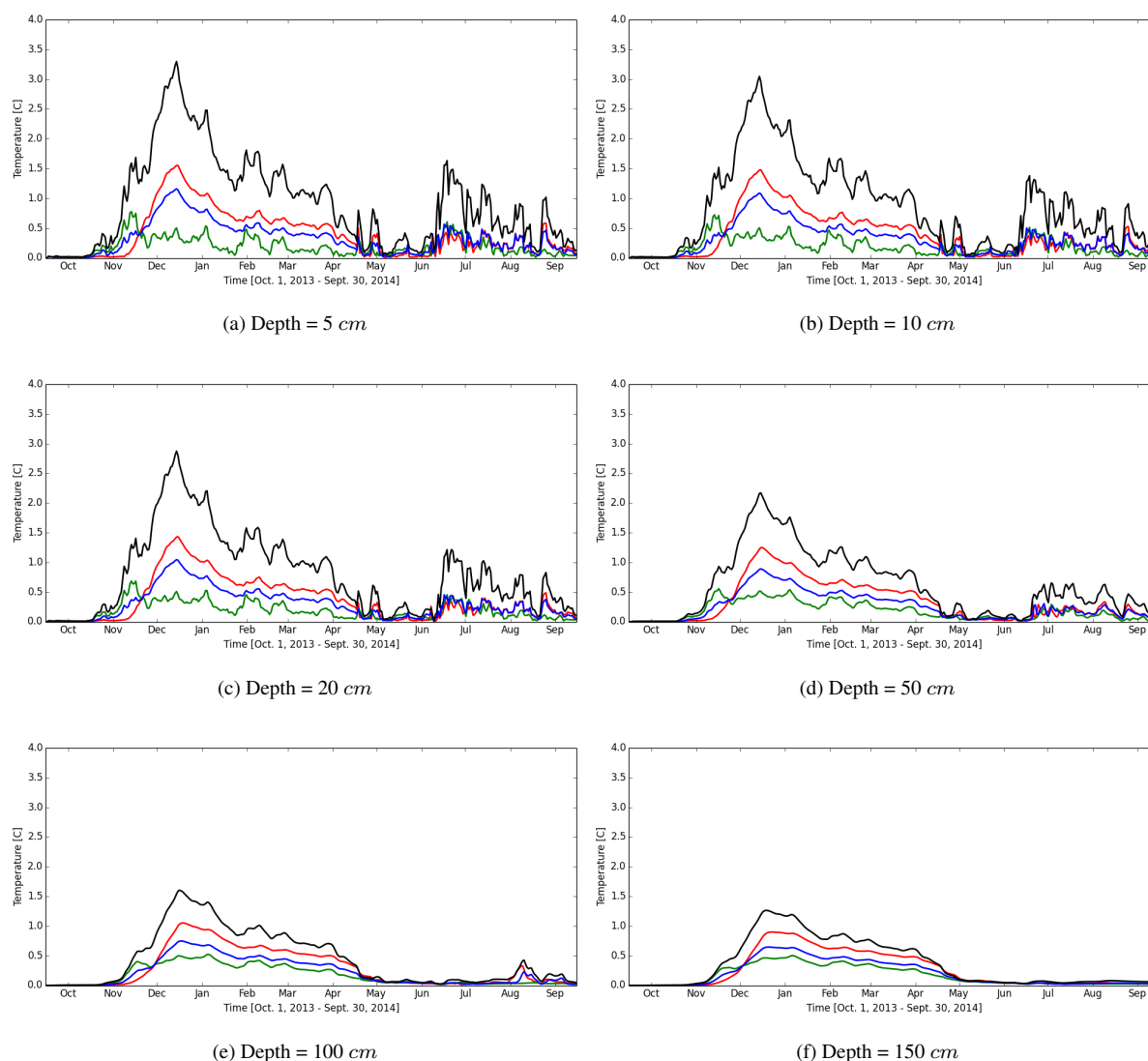
Figure 12. Spatio temporal variability (standard deviation) in simulated soil temperature at Site A.
Red, green and blue lines represent center, rim and trough respectively, and black line represent the standard deviation across the Site A.

Spatial variability in soil temperatures was observed in the simulations (Figures 8,9,10,11) arising in part due to three dimensional heat flow and heterogeneous subsurface structure and soil properties represented in the model. Simulated soil temperatures also show a seasonal pattern of spatial variability with high variability during the cold winter season and lower spatial variability during summer. Figure 12 shows time series of spatial variability (standard deviation) in soil temperature during the simulation period, showing strong seasonality, the magnitude of which is reduced at deeper soils.
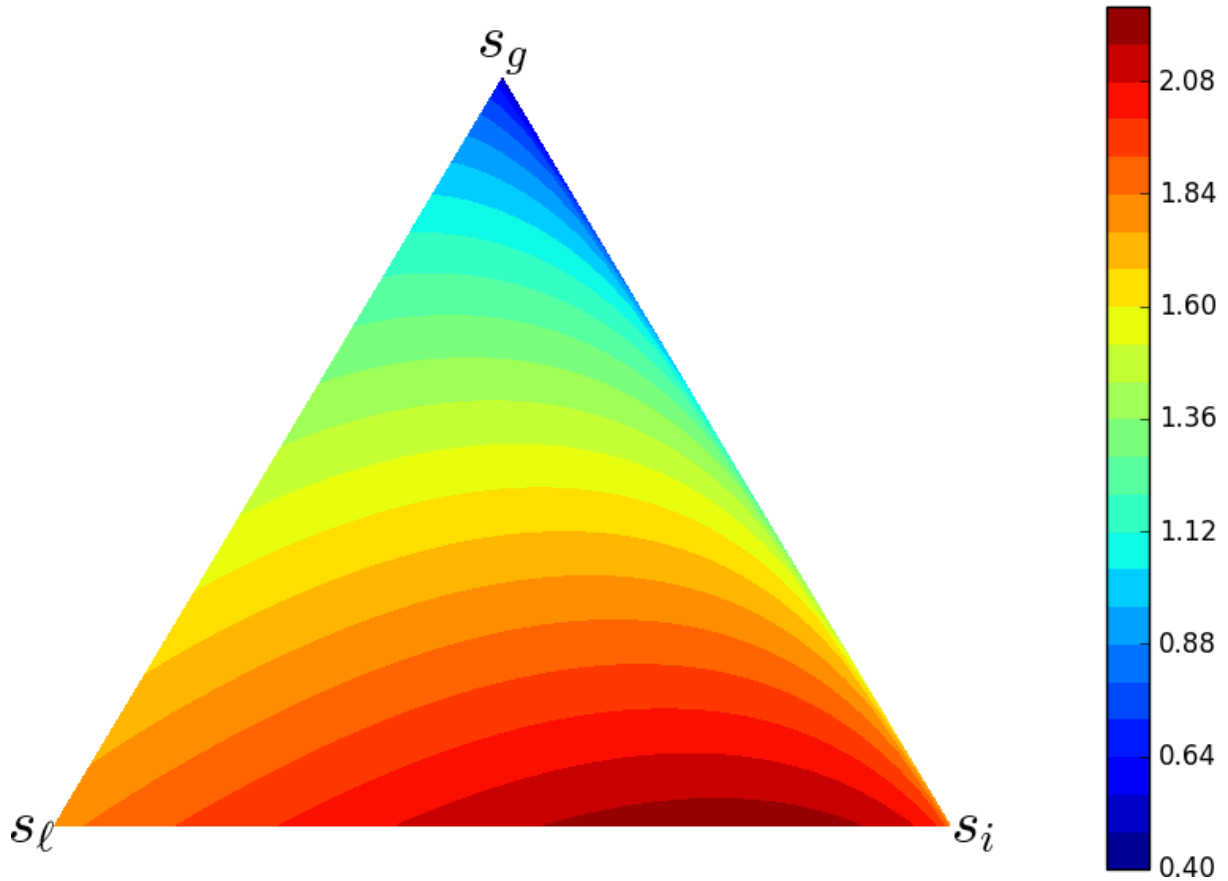
Figure 13. Model dependence of effective thermal conductivity on liquid (s_ℓ), ice (s_i) and gas phase (s_g) fraction of water

Heat flow in the permafrost soils which are frozen for a significant part of the year occurs primarily due to conduction. Thermal conductivity of the soil is sensitive to the temperatures and thus the fraction of water present in liquid vs ice phase (Equation (4)). Effective thermal conductivity (κ_{eff}) of the soil is higher during the winter months when almost the entire soil domain is in a frozen state (thus high ice saturation (s_i) and low liquid saturation (s_ℓ)), compared to summer months when active layer is in thawed state. Figure 13 shows the modeled dependence of effective thermal conductivity (κ_{eff}) on fraction of water present in liquid (s_ℓ)), ice (s_i) and gas (s_g) phases. Higher conductivity of the soil and thus higher conductive heat flows during the winter season in a heterogeneous soil domain leads to higher temperature variability in model simulations of the permafrost thermal regimes at our sites.

During the summer season, advective heat flow processes occur within the thawed soil layers. The study sites also receive liquid precipitation and thus infiltration during the summer season (Figure 2) which leads to vertical as well as horizontal flows in the thawed soil. For example, at Site A horizontal velocities are close to zero during the early summer (Figure 14(a)) when soil temperatures are close to freezing. After the ground has thawed, liquid precipitation events during summer (Figure 14(b,c))

Table 2. Model performance statistics at Site A compared to observed soil temperatures

Depth from surface [m]	Center			Rim			Trough		
	$RMSE$	R^2	$Bias$	$RMSE$	R^2	$Bias$	$RMSE$	R^2	$Bias$
0.02	0.97	0.98	-0.32	0.70	0.99	-0.09	0.81	0.99	0.10
0.05	0.73	0.99	-0.06	0.80	0.99	0.13	0.91	0.99	0.48
0.10	0.85	0.98	0.03	0.72	0.99	0.31	1.13	0.98	0.67
0.15	1.35	0.96	0.23	0.87	0.99	0.39	1.32	0.97	0.76
0.20	1.52	0.94	0.28	0.90	0.99	0.43	1.47	0.97	0.89
0.25	1.69	0.93	0.37	0.98	0.98	0.50	1.55	0.96	0.98
0.30	1.39	0.94	0.32	1.00	0.98	0.58	1.36	0.97	1.01
0.35	1.34	0.94	0.31	1.02	0.98	0.64	1.35	0.98	1.07
0.40	1.41	0.93	0.34	1.03	0.98	0.65	1.38	0.98	1.11
0.50	1.30	0.94	0.39	1.01	0.99	0.72	1.35	0.98	1.16
0.60	1.27	0.94	0.44	1.01	0.99	0.78	1.38	0.98	1.23
0.70	1.18	0.95	0.47	1.03	0.99	0.86	1.38	0.99	1.27
0.80	0.93	0.97	0.47	1.14	0.99	0.98	1.48	0.99	1.38
1.00	1.08	0.96	0.59	1.17	0.99	1.08	1.57	0.99	1.52
1.25	1.28	0.94	0.79	1.36	0.99	1.30	1.76	0.99	1.72
1.50	1.42	0.94	1.01	1.55	0.99	1.52	1.95	0.99	1.92

$RMSE$ = Root Mean Squared Error, R^2 = Coefficient of determination, $Bias = negative$ bias indicates cold bias in the model while $positive$ indicates a warm bias

lead to significant lateral flows. High elevation rim regions drain to the center and trough of the low-centered polygons. As ground thaws with the rise of summer temperature, significant lateral flow occurs even in the absence of rainfall events (Figure 14(d)).

4.3 Understanding the thermal regimes of polygonal tundra

Micro-topography of the polygonal tundra exerts critical controls on the flow of water and energy at local to regional scales which further influences the ecological and biogeochemical processes on the landscape. Surface processes (not explicitly modeled in our study) like vegetation and snow cover also play a critical role in regulating the subsurface thermal regimes through thermal insulation effects. In our modeling approach we represented the micro-topographic features Center, Rim and Trough across four low to transitional to high-centered polygons. PFLOTRAN successfully simulated the pattern of thermal regimes in Center, Rim and Trough across four sites A, B, C and D (Table 1).

- *Site A*: Site A is located in a poorly drained region dominated by low-centered polygons with low elevation centers, raised rims and troughs. Center areas are warmer than rim and trough areas while rims are coldest (Figure 8). Centers

Table 3. Model performance statistics at Site B compared to observed soil temperatures

Depth from surface [m]	Center			Rim			Trough		
	$RMSE$	R^2	$Bias$	$RMSE$	R^2	$Bias$	$RMSE$	R^2	$Bias$
0.02	0.99	0.98	0.06	0.54	0.99	-0.05	0.83	0.98	-0.07
0.05	0.83	0.99	0.34	0.50	0.99	-0.08	0.68	0.99	0.23
0.10	0.80	0.99	0.38	0.46	0.99	0.04	0.72	0.99	0.31
0.15	0.90	0.99	0.43	0.77	0.99	0.14	1.11	0.98	0.49
0.20	0.96	0.99	0.49	0.90	0.98	0.20	1.27	0.97	0.60
0.25	1.05	0.98	0.52	1.01	0.98	0.29	1.43	0.96	0.72
0.30	0.95	0.98	0.59	0.84	0.98	0.27	1.20	0.97	0.70
0.35	0.95	0.98	0.63	0.83	0.98	0.30	1.17	0.97	0.72
0.40	1.03	0.98	0.64	0.96	0.98	0.34	1.26	0.97	0.77
0.50	1.02	0.98	0.71	0.98	0.98	0.39	1.23	0.98	0.81
0.60	1.06	0.98	0.75	1.07	0.97	0.47	1.28	0.98	0.88
0.70	1.11	0.98	0.84	1.12	0.97	0.55	1.31	0.98	0.94
0.80	1.10	0.99	0.97	1.06	0.98	0.66	1.22	0.99	0.99
1.00	1.35	0.98	1.09	1.41	0.96	0.85	1.51	0.98	1.16
1.25	1.67	0.97	1.28	1.71	0.94	1.08	1.81	0.96	1.36
1.50	1.89	0.96	1.49	1.95	0.92	1.34	2.09	0.94	1.63

$RMSE$ = Root Mean Squared Error, R^2 = Coefficient of determination, $Bias = negative$ bias indicates cold bias in the model while $positive$ indicates a warm bias

in low-centered polygon are often innundated and relatively wet most of the year and support vegetation (mosses and sedges). Low elevation centers also receive higher snow cover. Vegetation and snow cover provide thermal insulation to the ground keeping the center region warmer compared to rim and trough. Dry rims with low vegetation cover and low snow accumulation (Figure 15) are most exposed to the winter temperatures and are thus the coldest.

5   – *Site B*: Site B is dominated by well drained high-centered polygons with relatively dry elevated centers and deep troughs. Vegetation in high-centered polygons are dominated by lichens, moss and dwarf shrubs. In contrast to the low-centered polygons, centers and dry-tundra graminoids have low vegetation and snow cover (Figure 15), are most exposed to the changes in air temperatures, and are thus colder than rim and trough which show relatively warmer soil temperature regimes during the winter. (Figure 9)

10   – *Site C*: Site C is located in an area of geomorphological transition from low to high-centered polygons, characterized as flat-centered polygons. They consist of shallow flat centers, deep troughs and raised rim regions. Soils in deep troughs are thermally insulated by higher snow cover (Figure 15) and thus show warmer soil temperature regimes compared to

Table 4. Model performance statistics at Site C compared to observed soil temperatures

Depth from surface [m]	Center			Rim			Trough		
	$RMSE$	R^2	$Bias$	$RMSE$	R^2	$Bias$	$RMSE$	R^2	$Bias$
0.02	0.90	0.99	-0.08	0.95	0.98	0.15	0.67	0.99	-0.04
0.05	0.80	0.99	0.18	1.84	0.96	0.50	0.69	0.99	0.29
0.10	0.63	0.99	0.12	1.23	0.98	0.35	0.78	0.99	0.34
0.15	0.85	0.99	0.21	0.78	0.99	0.31	1.09	0.98	0.57
0.20	0.93	0.98	0.26	0.80	0.99	0.37	1.11	0.98	0.62
0.25	0.98	0.98	0.29	0.80	0.99	0.36	1.16	0.98	0.68
0.30	0.81	0.98	0.29	0.86	0.99	0.41	1.06	0.98	0.70
0.35	0.87	0.98	0.32	0.83	0.99	0.41	1.12	0.98	0.80
0.40	1.03	0.97	0.38	0.80	0.98	0.40	1.16	0.98	0.84
0.50	0.96	0.97	0.42	0.75	0.99	0.42	1.13	0.98	0.91
0.60	0.91	0.98	0.44	0.73	0.99	0.46	1.15	0.99	0.98
0.70	0.87	0.98	0.53	0.73	0.99	0.52	1.17	0.99	1.06
0.80	0.78	0.99	0.64	0.77	0.99	0.56	1.20	0.99	1.14
1.00	0.93	0.99	0.80	0.86	0.99	0.76	1.34	0.99	1.29
1.25	1.13	0.99	1.02	1.02	0.99	0.95	1.58	1.00	1.52
1.50	1.35	0.99	1.27	1.23	0.99	1.19	1.81	1.00	1.76

$RMSE$ = Root Mean Squared Error, R^2 = Coefficient of determination, $Bias = negative$ bias indicates cold bias in the model while $positive$ indicates a warm bias

centers and rims (Figure 10). Center and rim regions show similar thermal regimes with centers being slightly warmer due to higher vegetation and snow cover.

– *Site D*: Site D is characterized as low centered polygons with no pronounced rims. Site D is wettest among the four study areas, with low elevation center areas that remain innundated for most of the summer season. While snow accumulation was fairly uniform (Figure 15) across the flat region, vegetation cover plays an important role. Wet centers supports rich vegetation, leading to a warmer soil temperatures as compared to the trough regions (Figure 11).

5 Model uncertainties and limitations

5.1 Why not to calibrate

Accurate simulation of permafrost thermal regimes requires the mechanistic representation of thermal hydrologic processes in the model. However, equally important is the accurate representation of subsurface structure and soil properties, model pa-

Table 5. Model performance statistics at Site D compared to observed soil temperatures

Depth from surface [m]	Center			Rim		
	$RMSE$	R^2	$Bias$	$RMSE$	R^2	$Bias$
0.02	0.87	0.99	-0.15	1.19	0.98	0.29
0.05	0.80	0.99	0.34	0.86	0.99	0.26
0.10	1.03	0.98	0.45	0.96	0.98	0.36
0.15	1.53	0.96	0.65	1.25	0.97	0.43
0.20	1.65	0.94	0.72	1.29	0.97	0.50
0.25	1.78	0.93	0.80	1.32	0.96	0.53
0.30	1.56	0.94	0.77	1.12	0.97	0.56
0.35	1.68	0.93	0.85	1.14	0.97	0.54
0.40	1.61	0.94	0.84	1.12	0.97	0.56
0.50	1.49	0.95	0.86	1.02	0.98	0.57
0.60	1.46	0.95	0.92	1.02	0.98	0.61
0.70	1.39	0.96	0.95	0.96	0.98	0.63
0.80	1.21	0.97	0.99	0.87	0.99	0.72
1.00	1.20	0.98	1.02	0.97	0.99	0.80
1.25	1.47	0.97	1.27	1.13	0.98	0.94
1.50	1.65	0.97	1.47	1.29	0.98	1.14

$RMSE$ = Root Mean Squared Error, R^2 = Coefficient of determination, $Bias = negative$ bias indicates
cold bias in the model while $positive$ indicates a warm bias

rameters and initial and boundary conditions. While PFLOTRAN was able to simulate the thermal hydrologic processes and match well the soil temperature observations at the sites across a range of polygonal landscape and micro-topography features, simulated soil temperatures show deviations from the observed temperatures at times. Simulated temperatures show warm bias in deep soils where data for soil characterization and properties are missing. Parameter calibration is a popular technique that

5   has been widely used in hydrologic modeling to determine model parameters and properties to optimize the model fit to target observations. The high resolution 3-D PFLOTRAN thermal hydrology model used in this study includes many degrees of freedom and parameters, which combined with complex non-linearity of hydrologic processes poses a complex high dimensional optimization problem. While a wide range of calibration approaches (Heuvelmans et al. (2006), Madsen (2000), Shafii and De Smedt (2009), Singh and Minsker (2008)) are available to determine optimal model parameters to fit the observed data (soil

10 temperatures in this study), we face the problem of non-uniqueness (equifinality). A diverse set of possible parameter values can lead to similar model performance (Beven and Freer (2001)). The issue of non-uniqueness is especially pronounced in tundra ecosystem due to poor availability of data and thus poor bounds on parameters which leads to a high degree of uncertainty in the models with or without calibration.

(a) June 17, 2014: P = 0.0 mm, GT_c = -0.137°C, GT_r = 1.199°C GT_t = -0.122°C

(b) June 23, 2014: P = 15.0 mm, GT_c = 1.435°C, GT_r = 1.743°C GT_t = 2.861°C

(c) June 30, 2014: P = 7.4 mm, GT_c = 9.780°C, GT_r = 4.134°C GT_t = 6.927°C

(d) July 06, 2014: P = 0.1 mm, GT_c = 10.513°C, GT_r = 4.435°C GT_t = 8.289°C
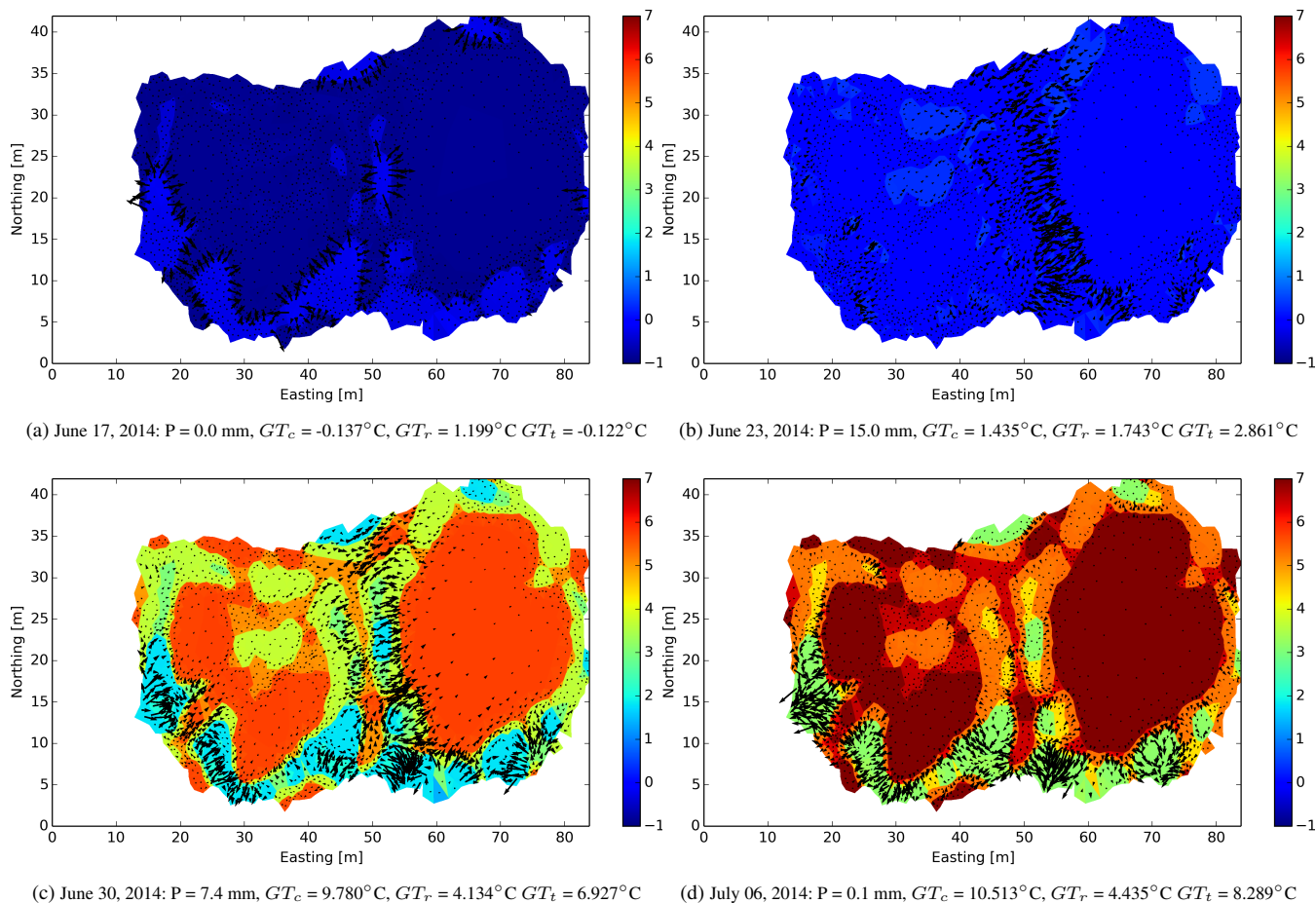
Figure 14. Lateral water flow velocity fields at Site A during early summer. In the horizontal cross section plot for Site A, background color shows the soil temperature distribution while the vector arrows show the magnitude and direction of lateral flow fields. (P = total daily precipitation, GT_c, GT_r, GT_t = mean ground surface temperature at center, rim and trough respectively.

While systematic calibration can help identify effective parameters for the model, transfer of parameters across models and modeling domains is difficult (Bárdossy (2007)). At our study sites, while calibration may compensate for lack of data, it does not improve our understanding of the system. In this study we choose not to calibrate the model parameters to achieve better fit with the observations, instead using the uncalibrated results to diagnose the potential model deficiencies and identify the characterization and data needed to better represent the real world in our simulations.

(a) Site A: rim, trough

(b) Site B: center, trough

(c) Site C: center, rim, trough

(d) Site D: rim
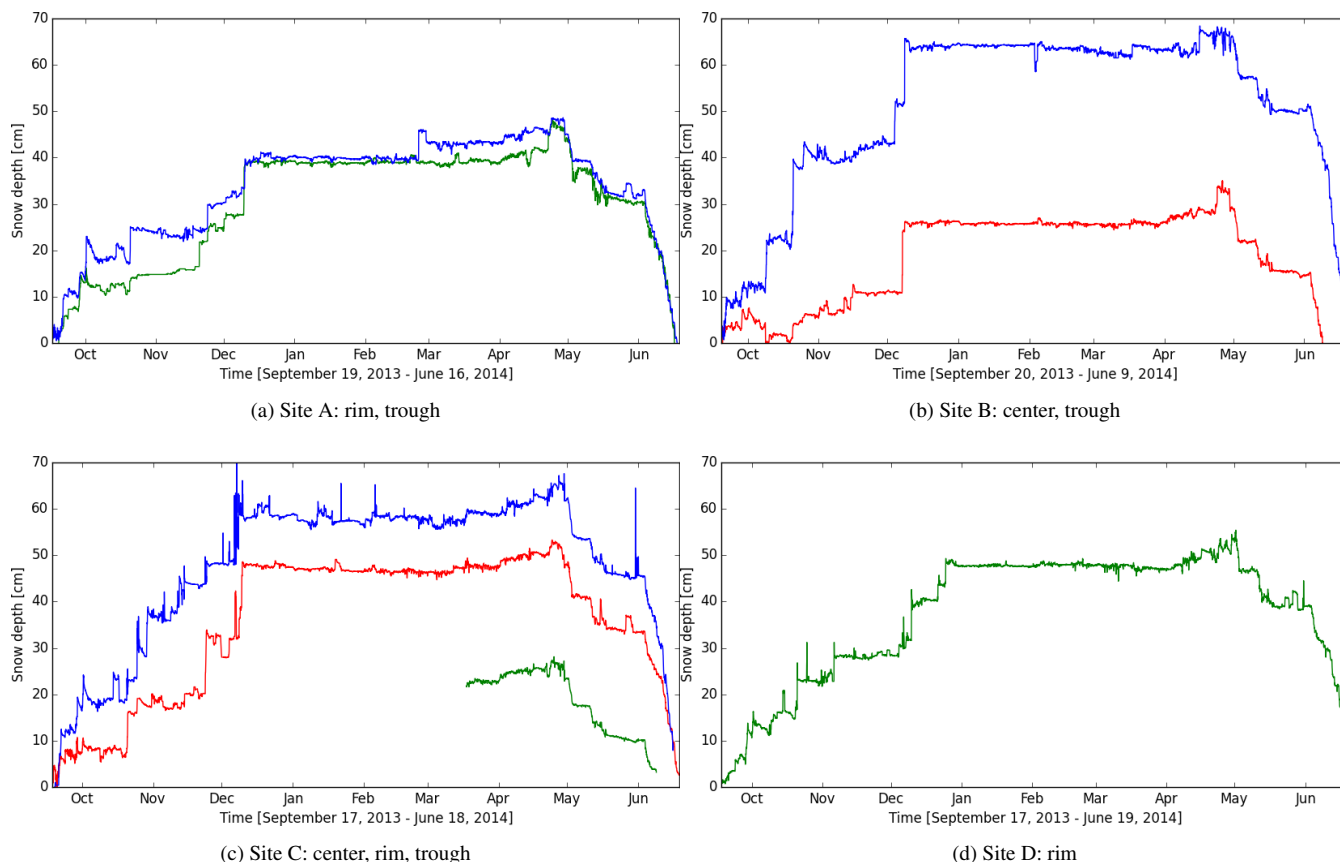
Figure 15. Observed snow depths at different topographic positions center (in red), rim (in green), trough (in blue) at our study sites (Hinzman et al. (2014a).

5.2 Identifying model and data gaps

While the agreement between modeled and observed simulated soil temperature demonstrates the ability of the model to simulated the thermal hydrologic processes in the polygonal tundra, disagreements help us identify the existing gaps in data and model.

5   Modeling results highlight the need for co-located measurements of soil thermal and hydraulic properties for accurate modeling of hydrologic processes. While most soil core observations, including these used in our study, are focused on the shallow active layer, characterization of deeper permafrost soils is essential for understanding the thermal regimes and potential changes expected under warming climate. Even during the winter season when soils are frozen, thermal dynamics may impact carbon fluxes (Zona et al. (2016)). Warmer than observed soil temperature in deep soils in our thermal periodic steady state solutions

10 are due to inaccurate soil characterization and poorly bounded boundary conditions at the bottom of the modeling domain. Heat flux observations in deep permafrost, while hard to measure, would help provide accurate bounds for the thermal hydrology

model. In addition to rainfall events (which was captured in our models), surface drainage processes provides inputs to the ground water system (not captured in our models). Surface drainage observations in the local catchments (not available to us) are needed to appropriately model and constrain this process.

While primary focus of the current study was to model and understand the subsurface thermal hydrology of polygonal tundra ecosystem, surface energy balance and snow processes also plays an important role. While beyond the current scope, efforts are underway within the NGEE–Arctic project to couple PFLOTRAN with a terrestrial biosphere model, the Community Land Model (CLM). The coupled CLM–PFLOTRAN model will provide an integrated treatment of surface and subsurface thermal hydrologic processes, and will be reported in future studies.

6 Summary and conclusions

Low-relief polygonal tundra ecosystems consist of micro-topographic features that controls the local scale hydrology. The water and energy flow patterns on the landscape in turn regulate biogeochemical processes and vegetation dynamics. The objective of this study was to develop an end-to-end modeling approach for landscape scale modeling of permafrost thermal hydrology of real world polygonal tundra sites, improving our ability to model and to understand the patterns of thermal regimes. Using the best available data for our study sites we developed techniques to characterize the polygonal microtopographic features and represent the heterogeneous soil hydraulic and thermal properties at the sites. These data sets were embedded within topography–following high–resolution meshes to simulate the thermal hydrologic processes in PFLOTRAN thermal hydrology model. We employed detailed surface meteorology and subsurface soil temperature observations from the site to simulate and analyze the thermal regimes at four representative sites in polygonal tundra ecosystem at the Barrow Environmental Observatory.

Our modeling–based study reveals the role of microtopographic features in regulating the permafrost thermal dynamics across heterogeneous polygonal tundra landscape. Simulation results at four sites across the polygonal tundra landscape demonstrate the effectiveness of the developed approach to model the thermal regimes. Thermal regimes of center, rim and trough features of polygonal tundra exhibit distinct patterns in low to transitional to high-centered polygon landscape, which are governed by the microtopography, surface and subsurface hydrology and surface processes (like air temperature, snow cover, and vegetation). Our PFLOTRAN–based modeling approach was able to successfully simulate these patterns at four study sites. In a warming world, wet low-centered polygon landscapes are expected to go through geomorphological change to drier high-centered polygonn landscapes. Modeling approach developed in this study would enable future investigations in impact of thermal hydrologic changes in these landscapes under projected climate scenarios. While beyond the scope of the current study, ongoing developments in biogeochemical modeling within PFLOTRAN (Tang et al. (2015)) in combination with our thermal hydrology model developments will also allow modeling of the terrestrial carbon cycle in this sensitive landscape under future warming scenarios.

We compared and validated the simulated soil temperatures against observations. While the models demonstrated the ability to simulate the soil temperature at shallow depths, the deviations from observations in deep soils highlights the need for better

soil characterization using deep cores in these ecosystems. Our study also highlights the need for co-located observations for accurate modeling and understanding of the tundra landscape. Model disagreements with the observations in this study may partially be due to use of soil properties from literature in absence of site–based measurements. Under the NGEE–Arctic project we are working with field scientists for improved co-located measurements. The modeling approach developed in this

5 study will allow accurate modeling of permafrost thermal hydrology and will help identify and guide the future observations required for improved modeling and understanding of the polygonal tundra ecosystem.

Acknowledgments

The Next Generation Ecosystem Experiments (NGEE) – Arctic project (http://ngee-arctic.ornl.gov/) is supported by the Office of Biological and Environmental Research in Department of Energy Office of Science. This manuscript has been authored by

10 UT-Battelle, LLC under Contract No. DE-AC05-00OR22725 with the U.S. Department of Energy. The United States Government retains and the publisher, by accepting the article for publication, acknowledges that the United States Government retains a non-exclusive, paid-up, irrevocable, world-wide license to publish or reproduce the published form of this manuscript, or allow others to do so, for United States Government purposes. The Department of Energy will provide public access to these results of federally sponsored research in accordance with the DOE Public Access Plan (http://energy.gov/downloads/doe-

15 public-access-plan). This research used resources of the Oak Ridge Leadership Computing Facility at the Oak Ridge National Laboratory, which is supported by the Office of Science of the U.S. Department of Energy under Contract No. DE-AC05-00OR22725.

Author contributions

JK designed the study and carried out the simulations. NC, GB, JK and RM developed the thermal hydrology model in

20 PFLOTRAN. NC and JK developed the meshing, characterization and parameterization techniques. CI collected and analyzed the soil cores and assisted with vegetation characterization. VR designed and maintained meteorological station and thermal sensors at the sites. JK led the analysis and writing of manuscript with contributions from NC, GB, RM, PT, CI and VR.

Appendix I: Model Reproducibility

Reproducibility, rigour, transparency and independent verification are cornerstones of the scientific method (Nature (2014)).

25 We document here model/software and computational platform used in the work reported in this study.

Software:
Subsurface thermal hydrology modeling was conduced using PFLOTRAN, which is an open source, state-of-the-art massively parallel subsurface flow and reactive transport code. PFLOTRAN (http://www.pflotran.org/) code is developed under GNU LGPL license and publicly available at https://bitbucket.org/pflotran.

```
PFLOTRAN version used:

Repository URL: https://bitbucket.org/pflotran/pflotran-dev

Changeset: 18ec488fc6ac
```

PFLOTRAN employs parallelization through domain decomposition using the MPI-based PETSc framework with *pflotran-dev* tracking the *git maint* branch of PETSc available through https://bitbucket.org/petsc/petsc.

```
PETSc version used:

Repository URL: https://bitbucket.org/petsc

Changeset: c41c7662de68b036bda6be236f939e8b55959cb0

Version: v3.5.2-137-gc41c766
```

Computational platform: All simulations were conducted on the *Titan Cray XK7* at Oak Ridge Leadership Computing Facility (https://www.olcf.ornl.gov/computing-resources/titan-cray-xk7/). GNU compilers were used to compile PFLOTRAN and

5 PETSc.

Appendix II: Data archiving and distribution

Model input files for all simulations reported along with the forcing data files, and computational mesh are publicly available through NGEE–Arctic long term data archive http://dx.doi.org/10.5440/1184018 (Kumar et al. (2016)). Summary outputs and statistics presented in various figures in this article are also available as part of the data collection. While the long term archiving

10 of complete PFLOTRAN simulation outputs reported here was not possible due to large data volume, they can be obtained by contacting the lead author.

Appendix III: Soil hydraulic and thermal properties

Table 6 shows the soil hydraulic and thermal properties used in our modeling study.

Table 6. Soil hydraulic and thermal properties used in the models

Parameter [Unit]	Moss	Organic	Mineral	Deep organic	Deep mineral	Data source
Porosity [–]	0.90	0.86	0.60	0.86	0.54	Hinzman et al. (1991)
Hydraulic conductivity [m/s]	1.94	1.04	0.376	1.08	0.14	Hinzman et al. (1991)
Bulk density [g/cm^3]	0.15	0.18	1.39	0.18	1.33	Hinzman et al. (1991)
VG Alpha (α) [1/Pa]	1.5×10^{-4}	1.5×10^{-4}	1.5×10^{-4}	1.5×10^{-4}	1.5×10^{-4}	–
VG Lambda (λ) [–]	0.23	0.95	0.33	0.95	0.33	–
Residual saturation [–]	0.05	0.34	0.20	0.34	0.20	–
κ_l [–]	0.45	0.43	0.8	0.43	0.8	Hinzman et al. (1998)
κ_i [–]	1.81	1.73	3.2	1.73	3.2	Hinzman et al. (1998)
κ_g [–]	1.81	1.73	3.2	1.73	3.2	Hinzman et al. (1998)
α_ℓ [–]	0.45	0.45	0.45	0.45	0.45	–
α_i [–]	0.97	0.07	0.97	0.97	0.97	–
Specific heat [$J/kg°C$]	1.04×10^4	8.65×10^4	2.36×10^3	3.19×10^2	2.46×10^3	–

References

Aleina, F. C., Brovkin, V., Muster, S., Boike, J., Kutzbach, L., Sachs, T., and Zuyev, S.: A stochastic model for the polygonal tundra based on Poisson–Voronoi diagrams, Earth System Dynamics, 4, 187–198, doi:10.5194/esd-4-187-2013, http://www.earth-syst-dynam.net/4/187/2013/, 2013.

5 Atchley, A. L., Painter, S. L., Harp, D. R., Coon, E. T., Wilson, C. J., Liljedahl, A. K., and Romanovsky, V. E.: Using field observations to inform thermal hydrology models of permafrost dynamics with ATS (v0.83), Geoscientific Model Development, 8, 2701–2722, doi:10.5194/gmd-8-2701-2015, http://www.geosci-model-dev.net/8/2701/2015/, 2015.

Bárdossy, A.: Calibration of hydrological model parameters for ungauged catchments, Hydrology and Earth System Sciences, 11, 703–710, doi:10.5194/hess-11-703-2007, http://www.hydrol-earth-syst-sci.net/11/703/2007/, 2007.

10 Beven, K. and Freer, J.: Equifinality, data assimilation, and uncertainty estimation in mechanistic modelling of complex environmental systems using the GLUE methodology, Journal of Hydrology, 249, 11 – 29, doi:http://dx.doi.org/10.1016/S0022-1694(01)00421-8, http://www.sciencedirect.com/science/article/pii/S0022169401004218, 2001.

Bockheim, J. G., Hinkel, K. M., and Nelson, F. E.: Soils of the Barrow region, Alaska, Polar Geography, 25, 163–181, doi:10.1080/10889370109377711, http://dx.doi.org/10.1080/10889370109377711, 2001.

15 Collier, N. and Kumar, J.: MeshMaker: Configurable Meshing Framework for Eco-Hydrology Models, Tech. Rep. ORNL/TM-2016/46, Oak Ridge National Laboratory, doi:10.5440/1237353, 2016.

French, H. M.: Thermokarst, pp. 186–215, John Wiley & Sons Ltd,., doi:10.1002/9781118684931.ch8, http://dx.doi.org/10.1002/9781118684931.ch8, 2007.

Hammond, G., Andre, B., Bisht, G., Collier, N., Karra, S., Kumar, J., Lichtner, P., and Mills, R.: PFLOTRAN: A Massively Parallel Reactive
20 Flow and Transport Model for describing Surface and Subsurface Processes, online, http://www.pflotran.org/, 2016.

Hammond, G. E., Lichtner, P. C., and Mills, R. T.: Evaluating the performance of parallel subsurface simulators: An illustrative example with PFLOTRAN, Water Resources Research, 50, 208–228, doi:10.1002/2012WR013483, http://dx.doi.org/10.1002/2012WR013483, 2014.

Heuvelmans, G., Muys, B., and Feyen, J.: Regionalisation of the parameters of a hydrological model: Comparison of linear regression models with artificial neural nets, Journal of Hydrology, 319, 245 – 265, doi:http://dx.doi.org/10.1016/j.jhydrol.2005.07.030, http://www.sciencedirect.com/science/article/pii/S0022169405003641, 2006.

Hinzman, L., Kane, D., Gieck, R., and Everett, K.: Hydrologic and thermal properties of the active layer in the Alaskan Arctic, Cold Regions Science and Technology, 19, 95–110, doi:10.1016/0165-232X(91)90001-W, 1991.

Hinzman, L., Romanovsky, V., Cable, W., and Busey, B.: Continuous Snow Depth, Intensive Site 1, Barrow, Alaska [Data], Next Generation Ecosystem Experiments Arctic Data Collection, Carbon Dioxide Information Analysis Center, Oak Ridge National Laboratory, Oak Ridge, Tennessee, USA, doi:10.5440/1163347, 2014a.

Hinzman, L., Romanovsky, V., Cable, W., and Busey, B.: Surface Meteorology, Barrow, Alaska, Area A, B, C and D [Data], Next Generation Ecosystem Experiments Arctic Data Collection, Carbon Dioxide Information Analysis Center, Oak Ridge National Laboratory, Oak Ridge, Tennessee, USA, doi:10.5440/1164893, 2014b.

Hinzman, L. D., Goering, D. J., and Kane, D. L.: A distributed thermal model for calculating soil temperature profiles and depth of thaw in permafrost regions, Journal of Geophysical Research, 103, 28 975–28 991, doi:10.1029/98JD01731, 1998.

Hobbie, S. E., Schimel, J. P., Trumbore, S. E., and Randerson, J. R.: Controls over carbon storage and turnover in high-latitude soils, Global Change Biology, 6, 196–210, doi:10.1046/j.1365-2486.2000.06021.x, http://dx.doi.org/10.1046/j.1365-2486.2000.06021.x, 2000.

Kane, D., Gieck, R., and L.C.Bowling: Impacts of surficial permafrost landforms on surface hydrology, in: Proceedings of the Eighth International Conference on Permafrost, edited by Philips, Springman, and Anderson, 2003.

Karra, S., Painter, S. L., and Lichtner, P. C.: Three-phase numerical model for subsurface hydrology in permafrost-affected regions (PFLOTRAN-ICE v1.0), The Cryosphere, 8, 1935–1950, 2014.

Kumar, J., Collier, N., Bisht, G., Mills, R. T., Thornton, P. E., Iversen, C. M., and Romanovsky, V.: Modeling the spatio-temporal variability in subsurface thermal regimes across a low-relief polygonal tundra landscape: Modeling Archive [Data], Next Generation Ecosystem Experiments Arctic Data Collection, Carbon Dioxide Information Analysis Center, Oak Ridge National Laboratory, Oak Ridge, Tennessee, USA, doi:10.5440/1184018, 2016.

Langer, M., Westermann, S., Muster, S., Piel, K., and Boike, J.: The surface energy balance of a polygonal tundra site in northern Siberia – Part 1: Spring to fall, The Cryosphere, 5, 151–171, doi:10.5194/tc-5-151-2011, http://www.the-cryosphere.net/5/151/2011/, 2011.

Liljedahl, A. K., Hinzman, L. D., Harazono, Y., Zona, D., Tweedie, C. E., Hollister, R. D., Engstrom, R., and Oechel, W. C.: Non-linear controls on evapotranspiration in arctic coastal wetlands, Biogeosciences, 8, 3375–3389, doi:10.5194/bg-8-3375-2011, http://www.biogeosciences.net/8/3375/2011/, 2011.

Madsen, H.: Automatic calibration of a conceptual rainfall–runoff model using multiple objectives, Journal of Hydrology, 235, 276 – 288, doi:http://dx.doi.org/10.1016/S0022-1694(00)00279-1, http://www.sciencedirect.com/science/article/pii/S0022169400002791, 2000.

Muster, S., Langer, M., Heim, B., Westermann, S., and Boike, J.: Subpixel heterogeneity of ice-wedge polygonal tundra: a multi-scale analysis of land cover and evapotranspiration in the Lena River Delta, Siberia, Tellus B, 64, http://www.tellusb.net/index.php/tellusb/article/view/17301, 2012.

Nature: Journals unite for reproducibility, Nature, 515, doi:10.1038/515007a, 2014.

Painter, S.: Three-phase numerical model of water migration in partially frozen geological media: model formulatoin, validation, and applications, Computational Geosciences, 15, 69–85, 2011.

Painter, S. and Karra, S.: Constitutive Model for Unfrozen Water Content in Subfreezing Unsaturated Soils, Vadose Zone Journal, 13, 2014.

Post, W. M., Emanuel, W. R., Zinke, P. J., and Stangenberger, A. G.: Soil carbon pools and world life zones, Nature, 298, 156–159, http://dx.doi.org/10.1038/298156a0, 1982.

Romanovsky, V. and Cable, W.: Subsurface Temperature, Moisture, Thermal Conductivity and Heat Flux, Barrow, Area A, B, C, D [Data],
5   Next Generation Ecosystem Experiments Arctic Data Collection, Carbon Dioxide Information Analysis Center, Oak Ridge National
Laboratory, Oak Ridge, Tennessee, USA, doi:10.5440/1126515, 2012.

Romanovsky, V. E., Smith, S. L., and Christiansen, H. H.: Permafrost thermal state in the polar Northern Hemisphere during the international
polar year 2007–2009: a synthesis, Permafrost and Periglacial Processes, 21, 106–116, doi:10.1002/ppp.689, http://dx.doi.org/10.1002/
ppp.689, 2010.

10 Shafii, M. and De Smedt, F.: Multi-objective calibration of a distributed hydrological model (WetSpa) using a genetic algorithm, Hydrology
and Earth System Sciences, 13, 2137–2149, doi:10.5194/hess-13-2137-2009, http://www.hydrol-earth-syst-sci.net/13/2137/2009/, 2009.

Singh, A. and Minsker, B. S.: Uncertainty-based multiobjective optimization of groundwater remediation design, Water Resources Research,
44, n/a–n/a, doi:10.1029/2005WR004436, http://dx.doi.org/10.1029/2005WR004436, w02404, 2008.

Skurikhin, A. N., Gangodagamage, C., Rowland, J. C., and Wilson, C. J.: Arctic tundra ice-wedge landscape characterization by ac-
15 tive contours without edges and structural analysis using high-resolution satellite imagery, Remote Sensing Letters, 4, 1077–1086,
doi:10.1080/2150704X.2013.840404, http://dx.doi.org/10.1080/2150704X.2013.840404, 2013.

Tang, G., Yuan, F., Bisht, G., Hammond, G. E., Lichtner, P. C., Kumar, J., Mills, R. T., Xu, X., Andre, B., Hoffman, F. M., Painter, S. L.,
and Thornton, P. E.: Using reactive transport codes to provide mechanistic biogeochemistry representations in global land surface models:
CLM–PFLOTRAN 1.0, Geoscientific Model Development Discussions, 8, 10 627–10 676, doi:10.5194/gmdd-8-10627-2015, http://www.
20 geosci-model-dev-discuss.net/8/10627/2015/, 2015.

Zona, D., Gioli, B., Commane, R., Lindaas, J., Wofsy, S. C., Miller, C. E., Dinardo, S. J., Dengel, S., Sweeney, C., Karion, A., Chang, R.
Y.-W., Henderson, J. M., Murphy, P. C., Goodrich, J. P., Moreaux, V., Liljedahl, A., Watts, J. D., Kimball, J. S., Lipson, D. A., and Oechel,
W. C.: Cold season emissions dominate the Arctic tundra methane budget, Proceedings of the National Academy of Sciences, 113, 40–45,
doi:10.1073/pnas.1516017113, http://www.pnas.org/content/113/1/40.abstract, 2016.